CEAS Space Journal (2022) 14:45–62
https://doi.org/10.1007/s12567-021-00366-4

ORIGINAL PAPER

Thrust measurements and evaluation of asymmetric infrared laser resonators for space propulsion

O. Neunzig[1] · M. Weikert[1] · M. Tajmar[1]

Received: 2 February 2021 / Revised: 10 March 2021 / Accepted: 13 April 2021 / Published online: 24 April 2021

Abstract
Since modern propulsion systems are insufficient for large-scale space exploration, a breakthrough in propulsion physics is required. Amongst different concepts, the EMDrive is a proposed device claiming to be more efficient in converting energy into propulsive forces than classical photon momentum exchange. It is based on a microwave resonator inside a tapered cavity. Recently, Taylor suggested using a laser instead of microwaves to boost thrust by many orders of magnitude due to the higher quality factor of optical resonators. His analysis was based on the theory of quantised inertia by McCulloch, who predicted that an asymmetry in mass surrounding the device and/or geometry is responsible for EMDrive-like forces. We put this concept to the test in a number of different configurations using various asymmetrical laser resonators, reflective cavities of different materials and size as well as fiber-optic loops, which were symmetrically and asymmetrically shaped. A dedicated high precision thrust balance was developed to test all these concepts with a sensitivity better than pure photon thrust, which is the force equivalent to the radiation pressure of a laser for the same power that is used to operate each individual devices. In summary, all devices showed no net thrust within our resolution at the Nanonewton range, meaning that any anomalous thrust must be below state-of-the-art propellantless propulsion. This puts strong limits on all proposed theories like quantised inertia by at least 4 orders of magnitude for the laboratory-scale geometries and power levels used with worst case assumptions for the theoretical predictions.

Keywords Laser resonators · EMDrive · Propellantless propulsion · Thrust balance

1 Introduction

Space propulsion encounters seemingly unattainable boundaries in their ability to fulfil humankind's ceaseless desire to explore the universe beyond our solar system. To lay the foundation for large-scale space exploration within our lifetime, a breakthrough in propulsion physics is required. Despite continuous advancements, modern propulsion technologies are limited in performance due to exponentially scaling propellant requirements according to the famous Tsiolkovsky rocket-equation, when facing enormous distances of interstellar missions. Solutions may hide in yet unknown interactions and origins of fundamental properties like mass and inertia themselves.

One proposed concept is the so-called EMDrive, which postulates to produce thrust using a microwave resonator inside a tapered cavity. Shawyer originally proposed that a difference in the radiation pressure between both ends of the cavity amplified by the cavity's quality factor Q is responsible for the effect [1]. The claimed force-to-power ratio of 1–100 μN/W is many orders of magnitude above classical radiation pressure with 0.033 μN/W, if we consider a laser producing thrust instead. This has been met with high scepticism, as it would violate basic conservation laws. Nevertheless, a number of theories as well as experiments have been proposed to support the EMDrive claim. A review of experiments and theories as well as a recent high-precision test can be found in our companion paper [2].

Taylor [3] suggested that the use of a laser resonator instead of microwaves may boost the produced thrust by orders of magnitude. Such a laser-EMDrive could also be

✉ M. Tajmar
martin.tajmar@tu-dresden.de

O. Neunzig
oliver.neunzig@tu-dresden.de

M. Weikert
marcel.weikert@tu-dresden.de

[1] Institute of Aerospace Engineering, Technische Universität Dresden, Marschnerstrasse 32, 01307 Dresden, Germany

much more compact and even simpler to build, which would be very interesting for potential applications. His analysis is based on the theory of quantised inertia by McCulloch, who claimed to explain the EMDrive as well as a number of other anomalies including dark matter [4, 5].

To test laser-EMDrives and related concepts, we developed a high-accuracy inverted counterbalanced double pendulum thrust balance, which allows operating laser devices with minimum drifts to reach a sensitivity in the sub-Nanonewton regime. This ensures that we have a resolution comparable to the photon thrust limit, which serves as the benchmark for propellantless propulsion. We tested a number of different concepts including configurations close to the idea of Taylor with a laser resonator of asymmetrical shape, reflective cavities as well as photon-loops with different geometries.

The paper starts with a summary of the theoretical predictions and gives an overview of our different experimental concepts. After an introduction of our thrust balance, we present the test results for all devices.

2 Theoretical predictions

Properties or the cause of inertia within our universe has never been understood in its entirety. Despite numerous efforts, neither its origin nor means to modify its properties were witnessed thus far. A new model to describe its underlying effects was proposed by McCulloch [6] within the theory of quantised inertia (QI) due to a Modified inertia Hubble-scale Casimir effect (MiHsC). In his model, inertia of an object emerges from dampening of Unruh radiation while it experiences acceleration. To explain the origin of inertia he assumes the formation of a relativistic Rindler horizon, appearing in the opposite direction to its acceleration that damps the Unruh waves thus creating an inhomogeneous distribution of radiation pressure. This process results in the effect we perceive as inertia with a modified inertial mass (m_i), including the standard inertial mass m, the speed of light c, the diameter of the observable universe Θ and the magnitude of the acceleration of the object compared to the surrounding matter $|a|$, and is given by

$$m_i = m\left(1 - \frac{2c^2}{|a|\Theta}\right) \tag{1}$$

With his theory, McCulloch provides alternative explanations for numerous physical topics including dark matter as well as the force generation of the EMDrive. In the laboratory, accelerations of regular masses are so low that this effect only appears at cosmic scales. However, this may change for radiation. His key assumption is that photons at the speed of light bounce back and forth in the cavity so fast, that $a \approx c^2/s$ with s being a representative length. This reduces the distance to the horizon Θ and the Unruh waves will be short enough to interact with the cavity walls. For a tapered cavity of length L and diameters d and D at the smaller and larger end, respectively, he expresses the force for the EMDrive [4] as

$$F_{EMDrive} = \frac{P \bullet Q \bullet L}{c} \bullet \left(\frac{1}{D} - \frac{1}{d}\right) \tag{2}$$

where P is the power into the cavity and Q the quality factor. Taylor [3] expanded this concept and expressed Q as a function of the wavelength λ, which leads to (correcting a wrong sign in his derivation)

$$F_{Taylor} = \frac{4\pi P \bullet L^2}{\lambda c \xi} \bullet \left(\frac{1}{D} - \frac{1}{d}\right) \tag{3}$$

with ξ as the cavity loss per oscillation or the energy lost divided by the energy initially stored. It immediately becomes clear that a short wavelength, e.g., of a laser compared to a microwave, should therefore lead to a larger force. His assumptions for an infrared laser with $\xi = 0.1$ and centimetre lengths give a force of 0.1 N for 1 W of input power [3], which is huge considering the force of just a few Nanonewtons for the same power as the classical radiation pressure force. He proposed a laser resonator with a dual-mirrored crystal, having a tapered cone shape like the EMDrive and being pumped by an array of laser diodes.

However, there may be a major error in both Eqs. 2 and 3 as we believe that this Q is not the same quality-factor as the one used by Shawyer for his EMDrive predictions [1]. The quality factor of a microwave resonator is a dimensionless parameter and describes the stored energy divided by energy lost per cycle. It characterizes the damping properties of the oscillator with low-energy loss in high-Q resonators and high energy-loss in low Q-resonators. But McCulloch understands Q as the equivalent number of times that the photons bounce back and forth within the cavity, "…the Q factor quantifies how many trips there are before the power dissipates" [4]. For optical cavities, the number of trips is the finesse divided by pi (2π for the number of round-trips) or the photon force amplification factor S. For two reflectivities R_1 and R_2 on each side of the cavity, this can be expressed as

$$S = \frac{\sqrt{R_1 R_2}}{1 - \sqrt{R_1 R_2}} \tag{4}$$

which is used to describes the force that pushes the mirrors apart from each other [7, 8]. That doubts Taylor's derivation and reduces the actual thrust predictions from quantised inertia in Eq. 2 (and invalidates Taylor's Eq. 3) if we set $Q = S$ as we believe McCulloch assumed. Using typical values for high-reflective mirrors, S can be in the range of

several hundreds, while the actual optical quality factor may be in the order of millions. Assuming that the length is at the same order of magnitude as the diameters of the cavity, this reduces the predicted forces to be 2–3 orders of magnitude above the photon thrust limit, which is still of major interest.

Assuming that we use photons that can produce the high accelerations necessary to interact with their environment, the theory then suggests two types of asymmetries, which can be tested: Mass asymmetries around the photons or different accelerations, e.g., by putting photons in a loop with different radii as a geometrical asymmetry on one side compared to the other one, as suggested by McCulloch and Diaz [9]. Both types can be mixed as well. We decided to test the following configurations:

Laser guiding into metal cavities with highly reflective surfaces: This closely resembles the original EMDrive concept. The cavities feature different radii as well as mass asymmetries around both ends. Copper and silver were used to test different force amplification values.
LED light inside a silver cavity with asymmetrical shape (called BART drive [9]).
Various laser resonators targeting Taylor's concept: We tested configurations with different mirror radii, crystals closer to one mirror as well as different wavelengths. Because the laser was present at one end only, it also features a mass asymmetry.
Photon-loops: We started with a classical symmetric photon loop and tested if a force appeared if we put a metal shield close to one end as suggested by McCulloch [10]. Then an asymmetrical loop was tested to directly obtain different photon accelerations on both ends. Again, a mass shield was put on both ends to see if that has an influence too.

Every theory described was subject of thorough investigations in our laboratory with a high accuracy thrust balance. The following chapters summarize the developed setups we used to account for the variety of theoretical predictions with laser resonators for space propulsion applications.

3 Experimental setup

Our main benchmark was to develop a test setup that has the sensitivity of the equivalent photon thrust for a given input power into the devices. To achieve this, we had to limit thermal drifts as much as possible as this is known to create balance deflections from center of gravity shifts or changes in the spring constants that can easily be misinterpreted as a real thrust. We therefore decided to limit the maximum laser power to one Watt, which translates into an equivalent photon thrust of $F = P/c = 3.3$ nN. Following the work from Taylor and the availability of commercial off-the-shelve components, we decided to target the near-infrared range.

The laser source of choice was a modular diode-pumped solid-state laser-kit by *Leybold* with a variety of optical components extended with highly reflective mirrors from *Laser Components*. The laser emits a fixed wavelength of 808 nm with adjustable power-levels between 0.01 W and 0.65 W with laser injection currents of up to 0.7 A supported by Peltier elements for temperature-controlled wavelength stabilization even in a vacuum environment. A collimator and converging focussing lenses handle parallelization of the bar-shaped beam. For high finesse resonator applications, especially the setups mentioned by Taylor, we utilized a Nd:YAG crystal with an attached coupling mirror to gain access to asymmetrically shaped beam patterns while converting the 808 nm into a wavelength of 1064 nm within the crystal. To confirm the active resonator by visualizing the 1064 mm only, a filter for the 808 nm wavelength was positioned within the setups. Concave and convex mirrors with reflectivities above 99.8% achieved the highest number of reflections.

Accurate predictions of the produced thrust required precise knowledge of the generated laser power in the test setup. For this purpose, we used a *Coherent LaserCheck* power-meter – a handheld measurement device for laser-power based on a calibrated silicon cell. With a maximum detectable power of 1 W and a minimum resolution of 0.01 µW for wavelengths between 400 and 1064 nm, it is well suited to ensure and inspect the laser power at different stages within each resonator. In addition, knowledge of the force amplification factor is required, which we computed using the reflection coefficients according to Eq. 4. For the photon-loop, this will be simply the number of turns of the fiber-optic cable.

3.1 Testing environment and thrust balance

Thrust measurements of the proposed setups in the vicinity of sub-micronewtons is a crucial objective when it comes to investigating and characterizing the underlying concept. Reliable measurement principles have to withstand doubts of any kind towards either the principle itself, the setup or most importantly measurement errors due to interactions with the test-environment. Especially newly developed thrust balances require enormous efforts to initially detect and minimize any undesired influences. Historically the single most popular measurement principle for electric propulsion systems is a torsion balance [11]. By measuring the deflection of a rigid spring-mounted beam onto which a thruster applies a torque, forces in the range of sub-micronewton can be detected. The simplicity of such devices is very appealing for high accuracy thrust measurements for space propulsion. Although this measurement principle is sophisticated and

offers possibly the highest resolution amongst previously utilized balances, it inherits very specific disadvantages, like any measurement principle so far, that constrain measurements depending on thruster mass and power consumption on the balance. The main difficulties in detecting forces with the required accuracy are center of mass shifts due to thermal expansion of mechanical components and magnetic interactions of power lines on the balance with external magnetic fields. Both of which lead to undesired deflections of the main beam and cause pseudo forces in measurements, which cannot be distinguished from real thrust.

We developed a new thrust balance with another measurement principle to counteract the disadvantages of torsional balances. The system of choice is presented in Fig. 1 with an inverted counterbalanced double pendulum. This measurement principle is based upon a deflecting frame onto which thrusters apply a force that linearly deflects a spring-mounted parallelogram, which is measured with an *attocube* laser interferometer. The device consists of two horizontal planes that rest on three aluminium beams for static determinateness. A total of nine torsional springs withhold relative motion between the components and ensure linear deflective behaviour. Thrust measurements rely on precise characterizations and calibration of the dependency between deflection and exerted force. Besides deflecting in another orientation, the center of mass-dependant deflective behaviour is the biggest difference between torsional balances and the double pendulum principle. The deliberate center of mass manipulation in the double pendulum balance enables an adjustability of measurement range and time for the balance to react on applied forces (reaction time). High resolution is acquired at the cost of high reaction time and vice versa. This property only counts for centre of mass shifts on the main beams connecting the upper and lower planes. Center of mass shifts on the planes itself do not interfere with measurements to a certain limit which leads to advantageous properties in measurements of high power/high weight thrusters.

Measuring small deflections of the balance as a result of applied thrust is very sensible towards any kind of stiff connections and wires to the deflecting frames. Every wire disturbs measurements by preventing deflections due to the stiffness of wire materials. To counteract this problem, the balance features electrical feedthroughs utilizing a metal alloy called Galinstan, which is liquid at room temperature and exhibits very low vapour pressure to operate in a vacuum environment.

Considering the prominent measurement errors due to magnetic interactions of power lines with external magnetic fields, especially Earths' magnetic field, the balance features twisted-pair as well as coaxial cables. Undesired vibrational excitation of the balance is decreased by Sorbothane sheets. Measurements with devices that produce excess heat on the balance at atmospheric pressure lead to buoyancy effects in close vicinity of the balance components that deflect the frame. Therefore, measurements take place in a cylindrical stainless-steel vacuum chamber to disable buoyant influences. We operated at a pressure of 10^{-2} mbar using an Edwards scroll pump which was sufficient for our purposes.

During initial measurements, a variety of additional influences were detected, caused by the laboratory environment and the balance components among each other. The predominant measurement error was caused by a magnetic interaction between wires on the balance and the permanent magnet of the pressure gauge, which was resolved by replacing and relocating the gauge. Additionally, the permanent magnets of the initially utilized passive eddy-current damping system repelled power-lines from the laser while operating. Replacing the passive system with an active damping

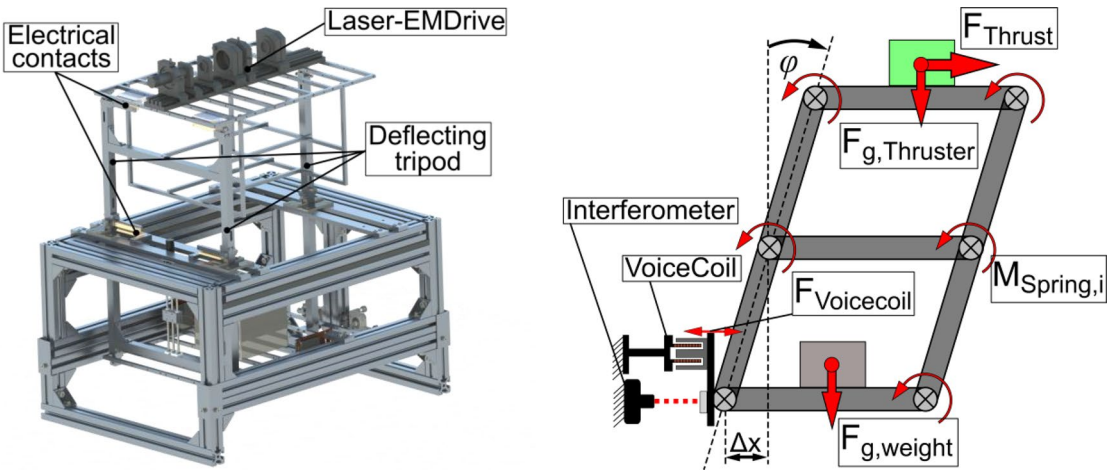

Fig. 1 Thrust Balance Schematic (Left: CAD-Model of the Inverted Counterbalanced Double Pendulum with the Taylor-Classic Setup, Right: Schematic Sketch of the Measurement Principle)

system eliminated this influence. Still another error source was surface tension between the pin contacts and the liquid metal feedthroughs, which depended on the applied current. This was mostly taken care of by either powering the laser from a separate structure off the balance, or using a battery powered laser. Some setups required a laser on the balance and power through the Galinstan contacts, which then had to be characterized before the actual thrust measurements.

Prior and after each individual thrust measurement, a calibration of the thrust balance is essential to ensure unaltered behaviour of the testbed. By applying forces of different magnitude with a voicecoil, we characterized the resulting deflections of the balance in the desired measurement range with statistical significance. Figure 2 illustrates an exemplary calibration process in two different measurement ranges. The graphs presented are consecutive measurements with different forces layered on top of each other. The voicecoil was activated for 50 s to determine the reaction time of the balance and resulting displacement that is monitored by the laser interferometer. An initial coarse calibration with forces of -0.9 µN to + 0.9 µN in steps of 0.1 µN (Fig. 2, Left) is followed by a fine calibration near the desired measurement range with forces between -0.08 µN and + 0.08 µN in steps of 0.01 µN (Fig. 2, Right). With a reaction time of 8 s, an operational time of 30 s for each laser-resonator-setup is sufficient to detect anomalous forces. Subsequently each data point is transferred into a linear fit of commanded force against measured displacement to verify linear deflective behaviour of the torsional springs in the measurement device (Fig. 3, left). Outcome of this process is the so-called calibration factor of 0.9682 µN/µm with a standard deviation of ± 0.0013 µN/µm. This value was used to convert the measured displacement into corresponding thrust forces.

As mentioned before, thermal effects may cause anomalies in measurement data that can be easily misinterpreted as real forces since they produce convincing thrust signatures.

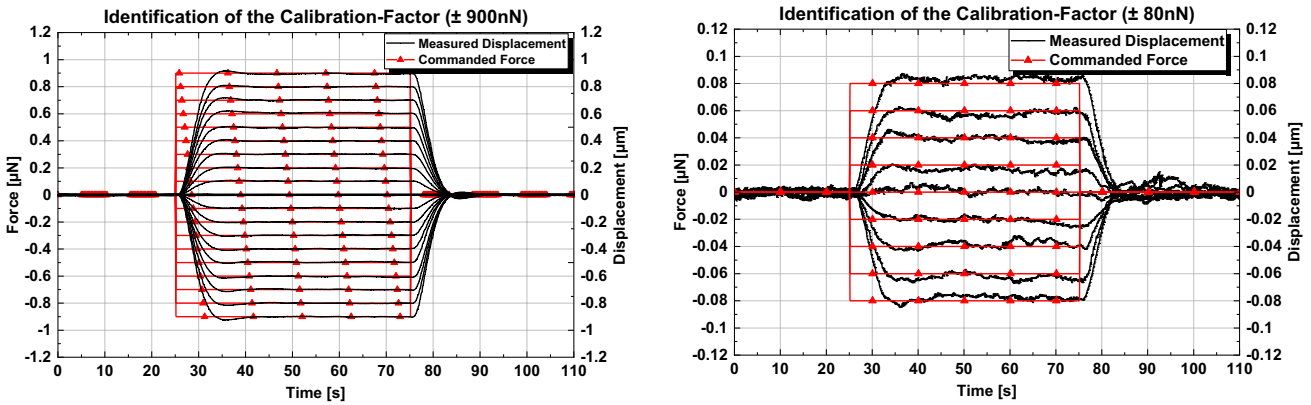

Fig. 2 Balance Calibration (Left: Rough Calibration through Commanded Forces with a Voicecoil, Right: Fine Calibration for the Desired Measurement Range)

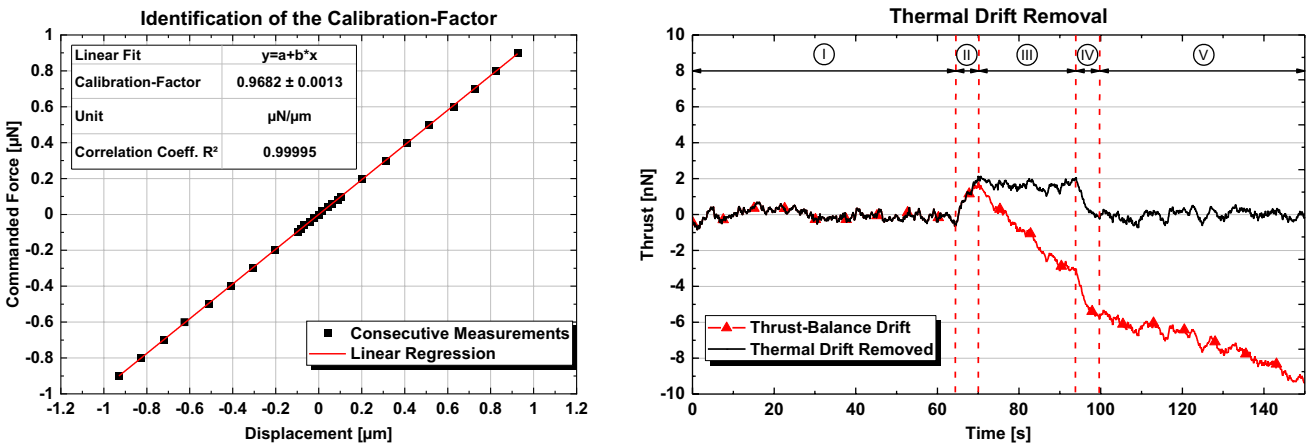

Fig. 3 Balance Characterisation (Left: Identification of the Calibration-Factor by a Linear Fit of Consecutive Data Points from the Commanded Forces, Right: Example for Software-Based Thermal Drift Removal)

Thermal drift in thrust measurements, especially in the range of Nanonewtons, is always present and superimposed on actual force-plateaus. As long as the drift is within a tolerable magnitude, we used software tools with LabView to automatically detect and remove them. To illustrate this process, consider the measurement in Fig. 3 (Right). The data shown is an average of 50 consecutive measurements from the effects of a laser beam fed into a beam trap. Each profile is divided into five sectors with fixed durations. Sector I and V characterize the balance behaviour prior and after feeding power into the resonator. Sector II and IV are ramping-periods that take the reaction time of the balance into account. Lastly, sector III contains the most meaningful information whether thrust is present. With linear fits of each sector, real thrust can be distilled from the raw measurement data that inherited a thermal drift of 9 nN for the measurement time of 150 s.

Using our voicecoil calibration technique, Fig. 4 shows an example to illustrate that the balance is sensitive enough to detect a Nanonewton of force as required. The data was averaged with several profiles to reduce noise and gain statistical significance. This was used throughout all measurements.

3.2 Beam trap

To confirm the sensitivity and thrust noise level of the balance, we utilized a device that absorbs the laser power to a negligible amount. This process simulates a thrust device with $S = 1$ by absorbing the photons on the measurement device and detecting the resulting force generation due to photon pressure. The beam trap *BTC30* by *Thorlabs* served for this purpose as it absorbs up to 5 W of laser power with wavelengths between 200 nm and 3 µm and has a backscatter of 0.005 as a fraction of entrance beam power. The opening aperture of 8 mm diameter ensures that the beam from our laser source with an estimated beam diameter of 2 mm is absorbed almost entirely. The absorbed energy generates heat within the beam trap that is transmitted to the thrust balance via thermal conduction and radiation. As mentioned before, thermal power generation on the balance may cause undesired measurement artefacts. We therefore stalled any heat transfer to the balance by adding thermal mass to the beam trap with pure copper blocks and a thermal radiation shield made from aluminium that is positioned around the beam trap except the beam entrance.

3.3 Metal cavities CC/CX—CC/CC—Circle, BART

Following the ideas of a geometrically and mass-asymmetric laser resonator, our first setup to be measured was a series of three different geometries made from solid copper. This material is well suited for reflective applications due to its theoretical maximum reflectivity of approximately 96% for wavelengths of 808 nm as well as its intrinsic property to serve as a heat sink for absorbed laser power preventing thrust balance heating. Our own measurements with the *Coherent* powermeter resulted in a reflectivity of 89%, probably due to the milled curved surface. Despite the high heat capacity, every copper cavity was encapsuled in an aluminium case, similar to the beam trap mentioned previously, to minimize heat radiation to the balance components. The geometries were chosen carefully to provide first insights into quantised inertia theory in a laboratory environment. Every cavity possesses a beam entrance with a diameter of 3 mm to ensure that the laser power enters unaffected. The cavities were polished prior to and in between thrust measurements to prevent a degradation in reflectivity. Detachable copper lids make sure that scattered laser beams are redirected into the resonator rather than expelled from the setup. All cavities are shown in Fig. 5.

The cavity described with CC/CX is characterized by two reflective surfaces with concave (CC) and convex

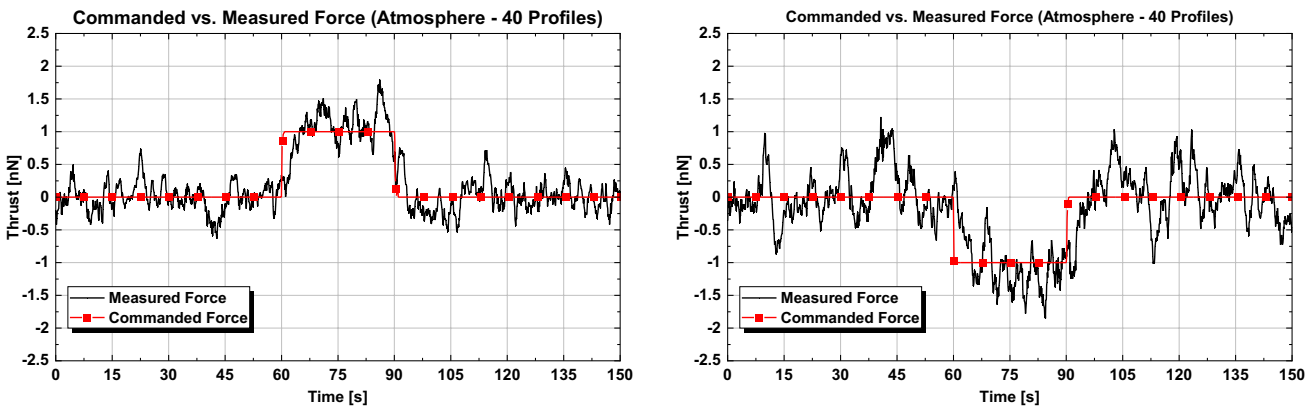

Fig. 4 Verification of the Voicecoil Calibration by Averaging 40 Consecutive Profiles with Commanded Forces of + 1 nN (Left) and -1nN (Right)

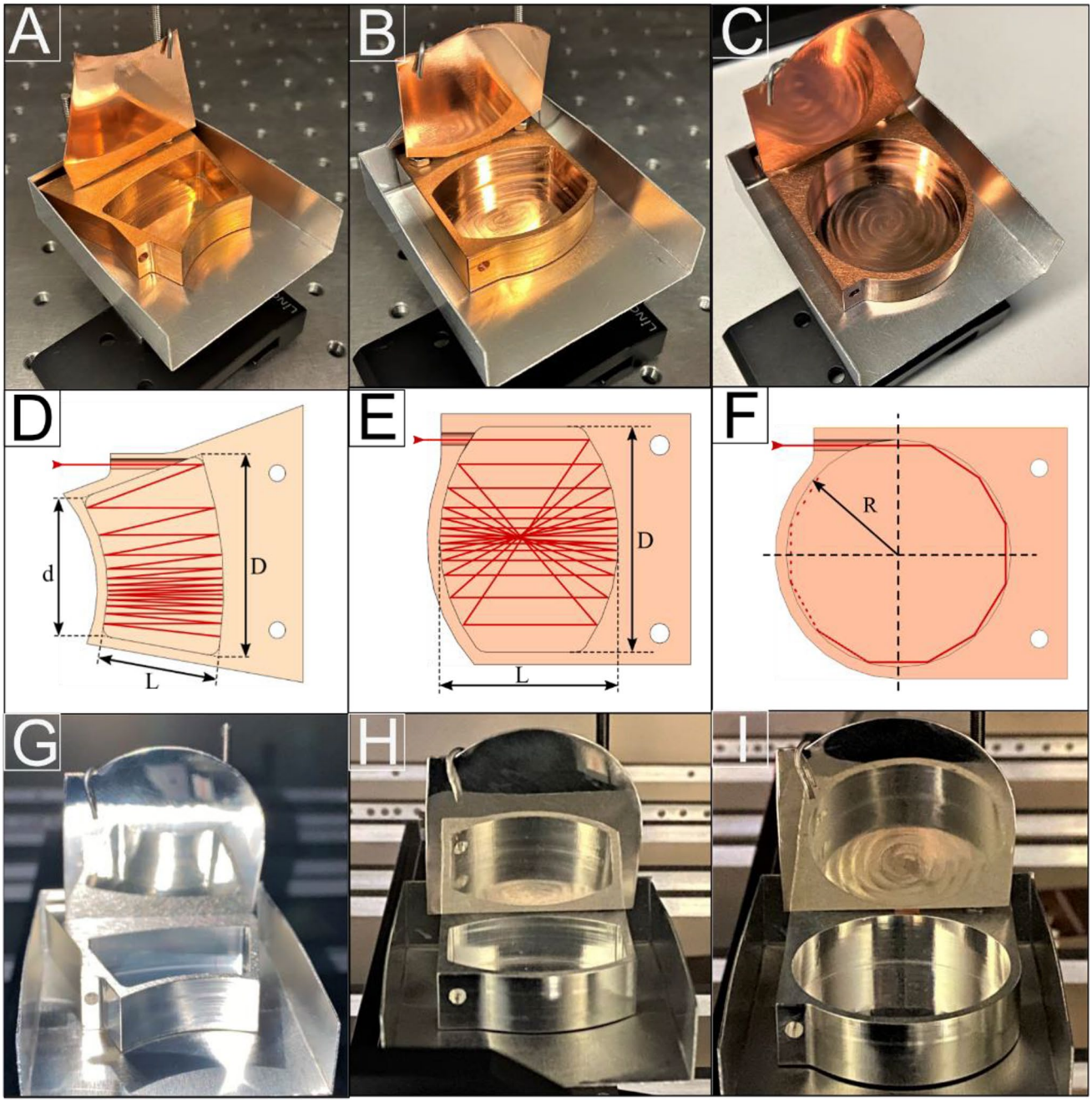

Fig. 5 Metal Cavities (A-C: Machine-Milled Solid Copper Cavities with Distinct Resonator Geometries. D-E: Schematic Sketch of Beam Patterns within the Cavities. G-I: Silver-Plated Cavities)

(CX) shapes. The curved surfaces are arranged in such a way that a laser is fed parallel to the axis of the entrance, where it is then reflected between the inner surfaces until being absorbed entirely. A sketch of the theoretical beam pattern is provided in Fig. 5d with the geometric dimensions of $d = 26$ mm, $D = 37$ mm and $L = 22$ mm. Here the geometric asymmetry is similar to an EMDrive tapered cavity but in 2D and the mass-asymmetry originates from the unequal copper mass distribution in front and behind the machine-milled resonator boundaries. These properties should lead to locally uneven damping of Unruh radiation of the reflecting photons and produce thrust according to quantised inertia.

In a similar manner, we manufactured the cavity described as CC/CC for both reflective surfaces characterized by concave shapes. The surfaces include a slight difference in radii to focus the beam and prevent it from escaping the resonator through the same pattern it entered the cavity. A difference

to the cavity CC/CX is an increase of mass asymmetry while changing the beam pattern as shown in Fig. 5 (E).

The last approach with copper resonators, described as Circle, involves a drastic change in beam pattern by guiding the laser along a circular trajectory while maintaining the mass asymmetry. Instead of back and forth reflections, the photons perform roundtrips with a defined radius R of 20 mm. This is actually similar to our later photon loop setups but with the Unruh shield as close as possible.

To directly test quantised inertia theory, we tried to increase the force amplification factor while maintaining the features, properties and even impurities due to the manufacturing process of each geometry. This was done by electroplating the copper cavities with a thin layer (< 1 µm) of pure silver to increase reflectivity of every surface to a theoretical maximum of 97.7% for infrared lasers at our 808 nm wavelength. Indeed, our own measurements gave a reflectivity of 97.5% close to the datasheet value. Simultaneously the number of reflections increases proportionally enabling a direct comparison between the same cavities and investigating the predicted linear dependency between thrust and number of reflections.

A very simple setup was suggested by Lucio and McCulloch and initial positive tests were reported by Komala [12] on a related metal cavity called the BART drive. Here, a 3 W LED diode was placed inside a closed silver cavity with a flat surface at one end and a zig-zag shape on the other, which leads to a significant increase in surface area and hence geometrical asymmetry. He claimed a thrust-to-power ratio of 1.75 µN/W. We decided to include this in our series of tests and developed a similar device as shown in Fig. 6 with an LED at a wavelength of 660 nm in the visible spectrum of light. We operated the LED at 0.77 W and 1.5 W optical power, which required currents that were similar to the one used for the photon-loops. The dimensions of the cavity were a diameter of 75 mm and a length of 100 mm. The zig-zag pattern had four spikes on the outside and three spikes on the inside over a height of 25 mm. We can express an equivalent diameter for the larger inner surface area on the right side, which is approximately 106 mm for our design. This can be viewed as a geometric asymmetry of 75 mm versus 106 mm for the cavity, which again resembles an EMDrive-like setup that can be computed using the theoretical prediction in Eq. 2.

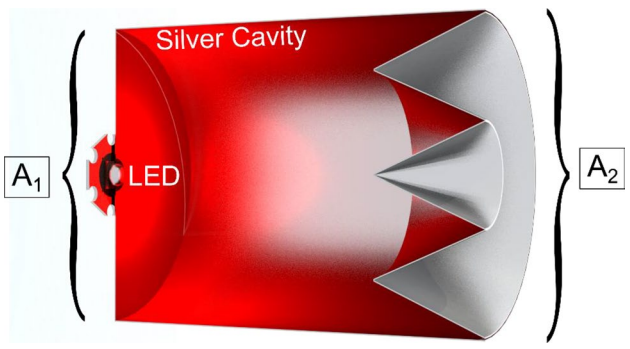

Fig. 6 Schematic Sketch of BART Drive in Sectional View (Rotationally Symmetric around Middle Axis) illustrating the Difference in Area $A_1 < A_2$

3.4 Taylor setups

Following the ideas of Taylor [3], we designed four different laser setups to test quantised inertia theory against high-finesse optical resonators in addition to the metal cavities. These particular setups utilized the modular components of the *Leybold* diode-pumped solid-state laser-source on a rigid rail with optomechanical mounts for quick and precise adjustments. The mirror mounts include adjustment screws to achieve a stable resonator by manual alignment and variation of its arrangement. The manufacturer ensured vacuum compatibility of the components as well as the laser source. Taylor's idea was to use a crystal in a tapered cone shape similar to an EMDrive, with reflective end surfaces that will create laser beam reflections inside that closely resemble the same shape. Such a crystal geometry is not commercially available, limiting us to a standard cylindrical shape. However, we were able to create laser resonators, where the beams indeed formed a tapered cone shape. In addition, we were able to introduce a variety of geometry and mass asymmetries, which we believe are even more asymmetrical compared to Taylor's design.

It is important to note, that the component holders and the rail provided a U-shaped cavity mass around all resonators. This does not represent a complete metallic enclosure as for the EMDrive, but at least a partial one. Although this was not part of Taylor's design and it is unclear if this is even necessary, our high sensitivity being 2–3 orders of magnitude better than any prediction should cover this aspect. In any case, the vacuum chamber acts as a full metallic enclosure too.

Accomplishing a resonator was difficult due to the fact, that infrared light is not visible to the naked eye. Three different approaches verified the desired operational mode during resonator setups and prior to measurements. The handheld powermeter mentioned previously monitored the laser power at different stages in between resonator components. In addition, optical confirmation was utilized too using an infrared-laser detection card, whose constituents are excited by the laser beam allowing visibility to the naked eye, and a camera that is sensitive to the infrared spectrum to confirm the operational modes. By operating the laser in pulsed mode, we could determine the typical decay time of the resonator using a *Leybold* photo diode and an oscilloscope,

which is a measure of the quality of the resonator and the time the photons spent within the cavity.

This was done in the following way: The laser with a wavelength of 808 nm enters the cavity where a Nd:YAG crystal converts it into 1064 nm. The mirrors in the cavity are reflective for 1064 nm and let the 808 nm pass through. Only a tiny amount of power from the 1064 nm, which is the resonating part, is passing through. After the cavity, a filter for the 808 nm is located such that only the 1064 nm part can be measured by the photo diode behind. By pulsing the laser, the decay time was measured by an oscilloscope. Our decay times for all setups were at a similar order of magnitude as the one given as an example in the manufacturer's handbook of 250 ns, which indicates the high quality of our resonator modes (equivalent to a Q of millions). In addition, the filter acted as a beam trap as most of the laser power was not allowed to pass through.

The following setups were implemented as illustrated in Fig. 7.

3.4.1 Taylor-light

To obtain the best thrust noise, we mounted the laser and collimator-lense assembly just next to the thrust balance on a separate platform eliminating potential electrical feedthrough problems. A Nd:YAG crystal with a diameter of 3 mm and a length of 5 mm was used as an entrance into the asymmetrical resonator. It converts the 808 nm into 1064 nm and has a flat mirror on its left end that is transparent for the incoming and reflective for the outgoing beam. At a distance of 75 mm, a concave mirror with a reflectivity of $> 99.8\%$ for 1064 nm, a diameter of 25 mm and a curvature with a radius of 100 mm is located. Widening of the beam by the crystal and the concave shape of the mirror ensures the tapered cone shape of the laser beam inside the resonator. This setup features a number of mass asymmetries:

Dielectric only on one side (5 mm out of 75 mm length). That is similar to what is claimed to be important for EMDrives [2]. In addition to different propagation speeds, this is also a strong mass asymmetry along the beam path. Setup Asymmetry: With the laser and collimator-lense assembly on one side only, the setup itself provides a strong mass asymmetry. In addition, the inserts for the crystal and the mirror on both ends are also dissimilar adding another asymmetry component.

3.4.2 Taylor halfway crystal

Here, the entrance is similar to Taylor-Light with the addition of another Nd:YAG crystal of diameter 10 mm and length 25 mm at a distance of 1 mm away from the first crystal. It features anti-reflective coatings on the end surfaces to ensure that the laser beam can pass through with minimal losses. The mirror on the right side has a 10 mm diameter with the same 100 mm curvature radius as in the setup above but with a higher reflectivity of $> 99.98\%$. The main goal of this setup was to increase the path length through a dielectric to roughly half the length of the resonator of length 50 mm, to investigate if this has any influence. In addition to the asymmetries listed above, the crystal and holder component now adds another important mass asymmetry along the laser path.

3.4.3 Taylor dual crystal

This setup is a combination of the two above. It is based on Taylor-Light, but with the larger Nd:YAG crystal included as well. This modifies again the path length of the laser through the dielectric ($5 + 25$ mm along a total length of 75 mm) with the larger diameter mirror at the right side that leads to a more pronounced conical beam shape.

3.4.4 Taylor classic

This configuration is as close as possible to Taylor's idea. It consists of a convex-concave mirror configuration with a resonator length of 65 mm to ensure the tapered cone shape laser beam with the large Nd:YAG crystal (10 mm diameter, 25 mm length) in between. The convex mirror was 25 mm in diameter with a curvature of 50 mm, a reflectivity of 99.7% and high transmissivity for the 808 nm wavelength to allow the laser beam to enter the resonator. The opposite side is occupied by a concave mirror with the same 25 mm in diameter but a curvature of 100 mm and a reflectivity of 99.8%. The conversion crystal was placed close to the entrance mirror to enhance asymmetry. Only in this setup, the laser was mounted together with all other optical components on the same rail as the correct alignment and tuning was very difficult and could not be achieved otherwise. This introduced artefacts from the currents passing through the feedthroughs that had to be taken into account.

3.5 Fiber-optic loop/photon-loop

Following the predictions of QI-Theory, we tested another setup that, in contrast to the metal-resonators described above, possesses an accurately defined number for the force amplification factor. By feeding a laser into a fiber-optic loop, the travelling photons should perceive a change in acceleration relative to their surrounding matter. Furthermore, the emerging Rindler horizon of an accelerated object may be substituted with an artificial horizon in the shape of an electrically conductive metal plate as illustrated Fig. 8. The plate was situated on one side of the fiber-optic loop, leading to an asymmetric dampening of the emerging Unruh

Taylor Light:

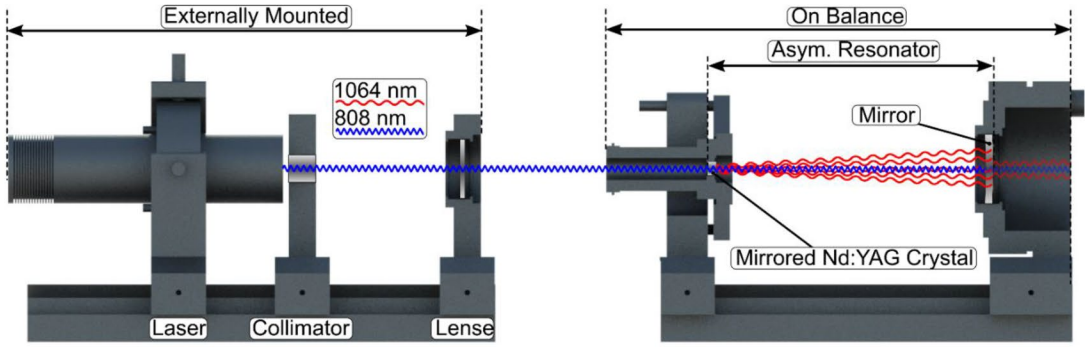

Taylor Halfway Crystal:

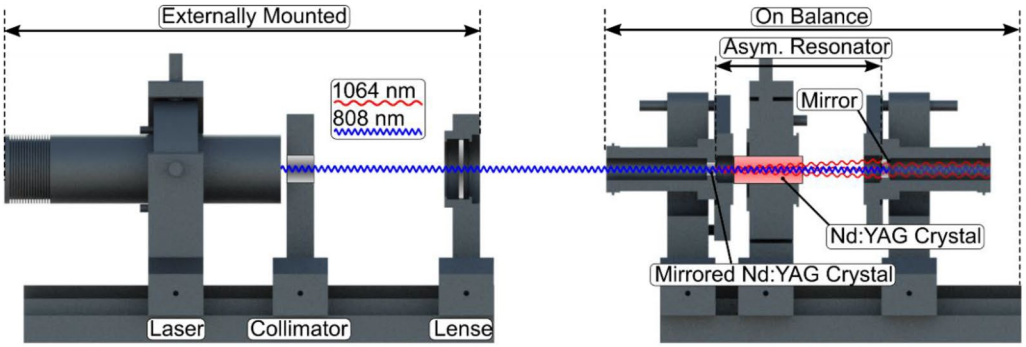

Taylor Dual Crystal

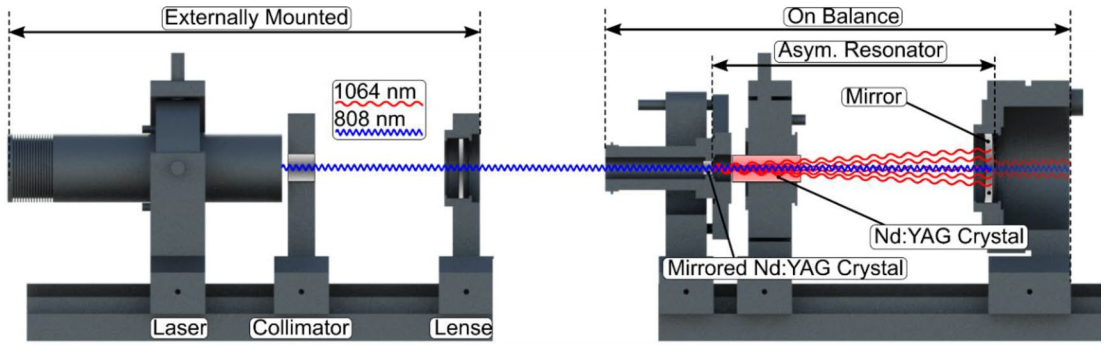

Taylor Classic:

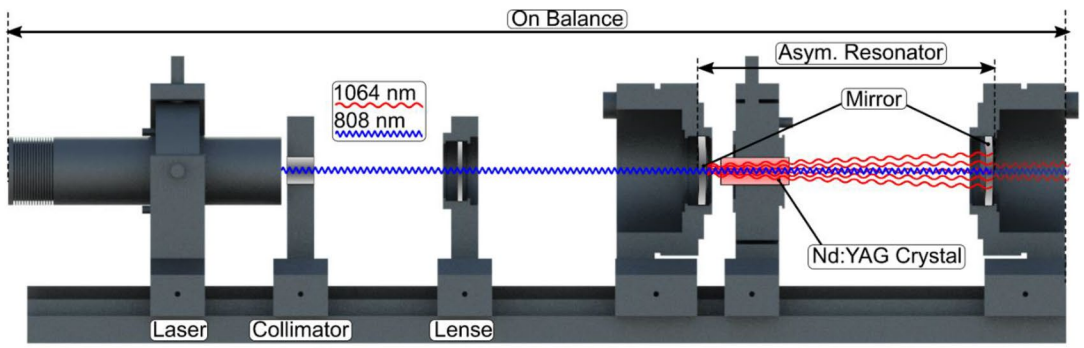

◂**Fig. 7** Illustrations of Taylor Setup Configurations (Light, Halfway Crystal and Dual Crystal have Laser mounted Externally, Classic has Laser Mounted on Balance)

radiation of the accelerated photons. To convert this idea into a physical test setup, we utilized 2.2 km of multimode fiber-optic cable for a coil diameter of 160 mm. We calculated the number of windings from its geometry resulting in at least 4330 although a value of 4000 was used for force predictions to account for uncertainties due to the coil thickness and to do a conservative estimate.

The same fiber-optic cable was reused on an asymmetric coil, which has two different radii. The support structure was 3D printed out of Polyetheretherketone (PEEK) with a radius of 70 mm on the big end and 40 mm on the small end. The center points of the radii are 150 mm apart from each other, resulting in an EMDrive-like cross sectional shape. With an accumulated number of at least 3300 windings for the same length, significant amounts of thrust should be generated. In addition, also in this asymmetric coil setup, an Unruh shield can be placed close to either radii.

Feeding the *Leybold* diode-laser beam into the fiber-optic cable was not possible as this would require a dedicated fiber-optic coupler which is difficult to tune. Instead, we replaced the diode-laser with a semiconducting laser that had a direct fiber-coupler attached for easy integration. It was supplied by *LUMILOOP* and featured a wavelength of 830 nm with up to 1 W of laser power starting from 50 mW. To prevent overheating in a vacuum environment, the laser was attached to an aluminium radiator with sufficient thermal mass. A *FTAPC1* beam trap from *Thorlabs* prevents photons at the end of the fiber from escaping the measurement-setup terminating a maximum power of 1 W.

The compactness of the semiconductor laser, which did not need separate control electronics like the *Leybold* laser, enabled to operate the whole assembly using a battery with six 18,650 Lithium-ion cells and a small power supply that was commanded via Bluetooth wireless communication. This eliminated all electrical feedthrough problems. Unfortunately, this battery solution was developed rather late in our program such that only the asymmetrical loop tests were done in this optimum configuration. The symmetrical loop used the same semiconductor laser but powered through the liquid metal feedthroughs, which resulted in some current-dependent offsets that had to be taken into account.

A picture of the actual setups is shown in Fig. 9.

3.6 Thrust measurements

A summary of all measurements can be found in Tables 1, 2, 3, 4, 5 including a comparison to predictions by QI-theory where applicable. We used the simple equation.

$$F_{QI} = \frac{P \bullet S}{c} \tag{5}$$

without geometry factors, as in most cases it is not exactly clear which length should be used. In any case, this gives the right order of magnitude and should provide a worst case thrust as geometric asymmetry and dielectric inserts should actually increase this value [4]. Simply put, we expect a force equivalent to photon thrust times the force amplification factor, calculated from the cavity reflectivities or the number of turns for photon-loops.

3.7 Beam trap

Our first measurements were used to get an independent verification of the thrust balance performance using a known force, the photon thrust from our laser, which was fired from a separate structure to avoid electrical feedthrough problems into the *BTC30* beam trap that was mounted on the balance. Each measurement was performed with at least two different power-levels to assess the power-scaling behaviour.

The acquired data resulted in thrust values of (0.32 ± 0.23) nN, (0.94 ± 0.31) nN and (1.64 ± 0.26) nN for measured laser power-levels of 109 mW, 292 mW and 497 mW, respectively. The values exactly match the calculated photon thrust of 0.36 mN, 0.97 nN and 1.66 nN based on their input power with total absorption (Table 1). Thrust measurement examples are shown in Fig. 10. This verified our ability of detecting forces with the fundamental physical mechanism of momentum exchange with photons ($S = 1$).

3.8 Metal cavities CC/CX—CC/CC—Circle, BART

As we are shooting with the externally mounted laser into the metal cavities mounted on the balance, we expected to see a force amplification factor with respect to classical photon thrust of 9 and 39 for the copper and silver cavities respectively. All force measurements for the CC/CX, CC/CC and Circle setups are summarized in Table 2 for three different power levels. They show an excellent agreement with classical photon thrust and no anomalous force as predicted by QI.

However, during our test campaign we encountered an interesting problem that produced a false-positive thrust effect, which is important to note for possible replication efforts. After finishing measurements with copper resonators, we electroplated the same cavities with pure silver to increase their reflectivity. First measurements of the silver-coated cavity CC/CX indeed showed a force that was 50% higher compared to the equivalent photon thrust. Due to suspicious on- and off-delays in the occurred force plateaus compared to the fast reaction time of the balance, we suspected a measurement error of unknown origin at that time.

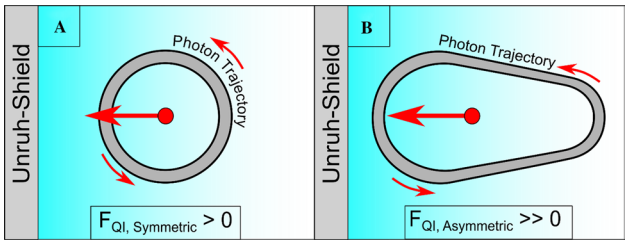

Fig. 8 Photon-loop Configurations (A: Symmetric Fiber-optic Loop with Unruh Shield, B: Asymmetric Fiber-optic Loop with Unruh Shield Close to its Bigger Radius)

Taking all ideas into account, we identified, that the manufacturer responsible for the silver coating did not mention a transparent film on top of the silver layer to protect it against degradation. It turned out that the laser locally heated and vaporized the non-vacuum compatible layer that increased the measured thrust and was responsible for the spurious delays of the signal. We detected this error by noticing a pressure increase within the chamber during and after laser operation, monitored by the pressure gauge. The solution to this problem was heating the cavity in an oven at 200° for several hours to destroy the protective layer. The resulting thrust measurements showed no anomalous forces above

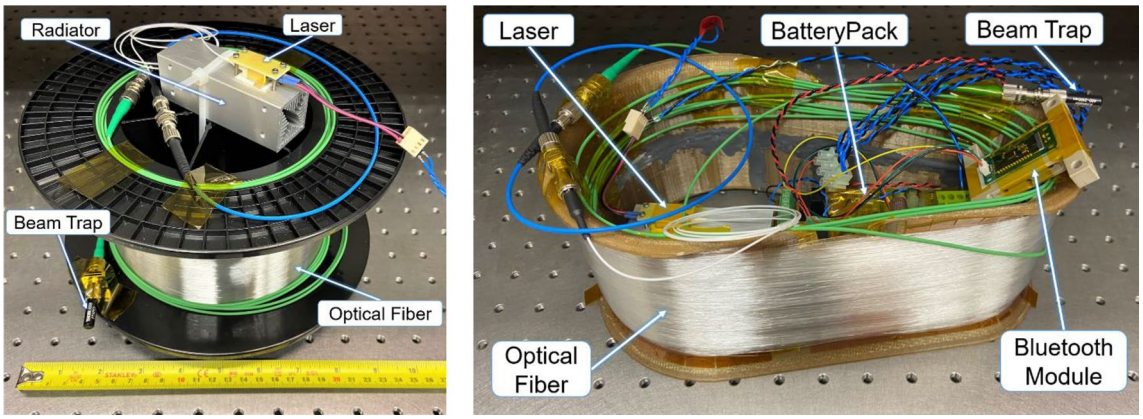

Fig. 9 Photon-loop Setup during Tests (Left: Symmetric Fiber-optic Loop with a Semiconducting Laser-Diode, Right: Asymmetric Fiber-optic Loop with Electrical Components)

Table 1 Beam trap measurements

Setup	Measured Power	Classical Photon Thrust (S = 1)	Measured Thrust
Beam Trap	109 mW	0.36 nN	(0.32 ± 0.23) nN
	292 mW	0.97 nN	(0.94 ± 0.31) nN
	497 mW	1.66 nN	(1.64 ± 0.26) nN

the equivalent photon pressure. Thrust measurements of the silver cavity for two power levels are shown in Fig. 11, where the laser current indicates when the laser was on. No anomaly beyond classical photon thrust and excellent balance response can be seen in this case.

The BART silver cavity measurements are summarized in Table 3. As the LED was mounted inside the cavity, classically one would not expect any thrust at all, which

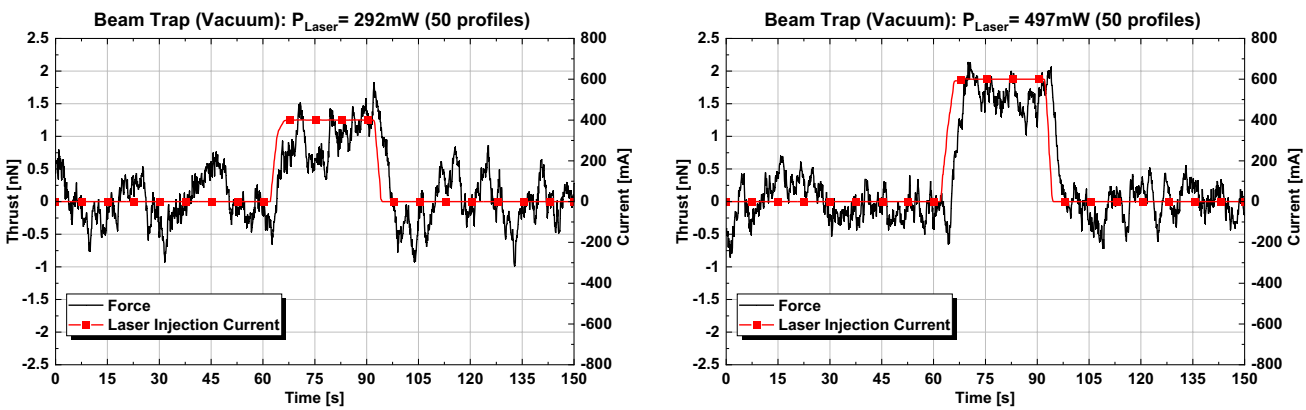

Fig. 10 Thrust Measurement of the Beam Trap *BTC30*

Table 2 Metal cavity measurements

Setup	Surface Material	Force Amplification Factor (S)	Measured Power (P)	QI Force Prediction (F = PS/c)	Classical Photon Thrust (S = 1)	Measured Thrust
Concave/Convex (CC/CX)	Copper	9	109 mW	3 nN	0.36 nN	(0.39 ± 0.19) nN
			292 mW	8 nN	0.97 nN	(1.02 ± 0.15) nN
			497 mW	14 nN	1.66 nN	(1.67 ± 0.16) nN
	Silver	39	292 mW	38 nN	0.97 nN	(1.08 ± 0.18) nN
			497 mW	65 nN	1.66 nN	(1.73 ± 0.24) nN
Concave/Concave (CC/CC)	Copper	9	109 mW	3 nN	0.36 nN	(0.40 ± 0.15) nN
			292 mW	8 nN	0.97 nN	(1.03 ± 0.14) nN
			497 mW	14 nN	1.66 nN	(1.65 ± 0.22) nN
	Silver	39	292 mW	38 nN	0.97 nN	(1.28 ± 0.34) nN
			497 mW	65 nN	1.66 nN	(1.76 ± 0.28) nN
Circle	Copper	9	109 mW	3 nN	0.36 nN	(0.34 ± 0.28) nN
			292 mW	8 nN	0.97 nN	(1.12 ± 0.25) nN
			497 mW	14 nN	1.66 nN	(1.71 ± 0.27) nN
	Silver	39	292 mW	38 nN	0.97 nN	(1.13 ± 0.27) nN
			497 mW	65 nN	1.66 nN	(1.89 ± 0.24) nN

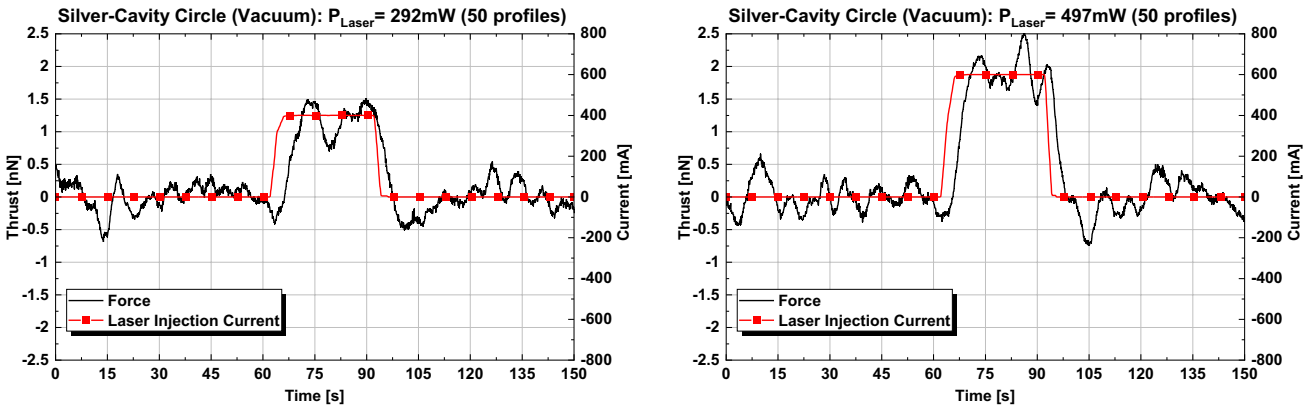

Fig. 11 Thrust Measurement of the Silver Cavity "Circle"

Table 3 LED cavity (BART drive) measurements

Setup	Measurement Influence	Power (P)	Classical Photon Thrust (S = 1)	Measured Thrust
BART Drive	Liquid Metal Contacts	770 mW	2.57 nN	(0.13 ± 1.35) nN
		1540 mW	5.14 nN	(0.22 ± 4.13) nN
		497 mW	1.66 nN	(1.95 ± 0.41) nN

is indeed what we measured. At 1.54 W of optical LED power, the expected thrust from the claimed measurement would have been 2700 nN [12], however we measured (0.22 ± 4.13) nN, ruling out any anomalous thrust by 4 orders of magnitude.

3.9 Taylor setups

Thrust measurements of the Taylor setups required increased effort due to their vulnerability against misalignments of the optical axis. A precise parallelisation of both optical axes

was achieved by varying the adjustment screws while monitoring the infrared beam with a camera. A resilient resonator mode was achieved when an indicator occurred on the infrared detection card (Fig. 12).

A summary for all configurations is given in Table 4. The first three Taylor setups (Light, Dual Crystal and Halfway Crystal) were straightforward as the laser was mounted externally from the balance. As the laser power was mostly absorbed within the resonator and the filter at the end of the rail, the classical prediction would be again to measure pure photon thrust. The much higher reflectivities of the commercial mirrors with respect to our own polished metal surfaces resulted in an order of magnitude higher force amplification factors, which was varying between 500 and 908 for the setups. These values are equivalent to actual measurements with similar mirrors [7, 8]. Again, our data showed only classical photon thrust ruling out theoretical predictions by three orders of magnitude. An example for Taylor-Light is shown in Fig. 13.

For the Taylor-Classic configuration, the laser was mounted on the main balance rail. Therefore, we had to take the influence from the current passing through the liquid metal contacts into account. This was done by first blocking the laser to have a zero-thrust reference, and second without the laser block. Our results in Table 4 show that the feedthrough influence is very small at around 6–7 nN for 500 mW. Still this was above our photon thrust threshold. By taking the difference between both measurements we get a null result below photon thrust as expected. No anomaly was seen also in this configuration, which is as close as possible to Taylor's original idea. The thrust measurements with blocked, unblocked and differential configurations are shown in Fig. 14.

3.10 Symmetric- and asymmetric fiber-optic loops

The fiber-optic loops finalized our efforts of investigating force generation in photon-based resonators. Specifically, the known number of windings is important for a correct thrust prediction using QI-theory.

First, the symmetrical circular fiber-optic coil was tested. We used the coil as shipped by the manufacturer to ensure

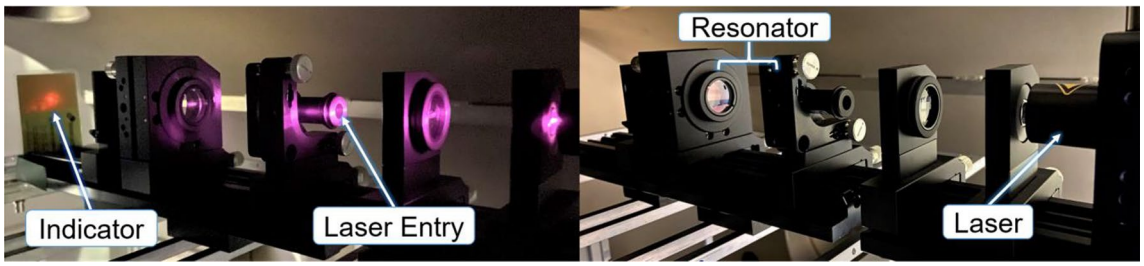

Fig. 12 Taylor-Light Setup with an Active Resonator Configuration indicated by the Infrared Detection Card (Note: Laser is Mounted on a Separate Rail external to the Balance)

Table 4 Taylor-like laser resonator measurements

Setup	Measurement Influence	Dielectric	Force Amplification Factor (S)	Measured Power (P)	QI Force Prediction (F = PS/c)	Classical Photon Thrust (S = 1)	Measured Thrust
Taylor Light	–	No	500	292 mW	487 nN	0.97 nN	(1.03 ± 0.14) nN
				497 mW	828 nN	1.66 nN	(1.78 ± 0.31) nN
Taylor Dual Crystal	–	Nd:YAG Crystal	500	292 mW	487 nN	0.97 nN	(1.14 ± 0.57) nN
				497 mW	828 nN	1.66 nN	(1.62 ± 0.15) nN
Taylor Halfway Crystal	–	Nd:YAG Crystal	908	292 mW	885 nN	0.97 nN	(0.97 ± 0.12) nN
				497 mW	1505 nN	1.66 nN	(1.75 ± 0.32) nN
Taylor Classic	Liquid metal contacts; Laser Blocked	Nd:YAG Crystal	0	292 mW	0 nN	0.97 nN	(3.98 ± 0.61) nN
				497 mW	0 nN	1.66 nN	(6.82 ± 1.53) nN
	Liquid metal contacts		624	292 mW	608 nN	0.97 nN	(4.41 ± 0.87) nN
				497 mW	1035 nN	1.66 nN	(6.64 ± 1.32) nN
	None (Differential)			292 mW	608 nN	0.97 nN	(0.43 ± 0.87) nN
				497 mW	1035 nN	1.66 nN	(0.18 ± 1.53) nN

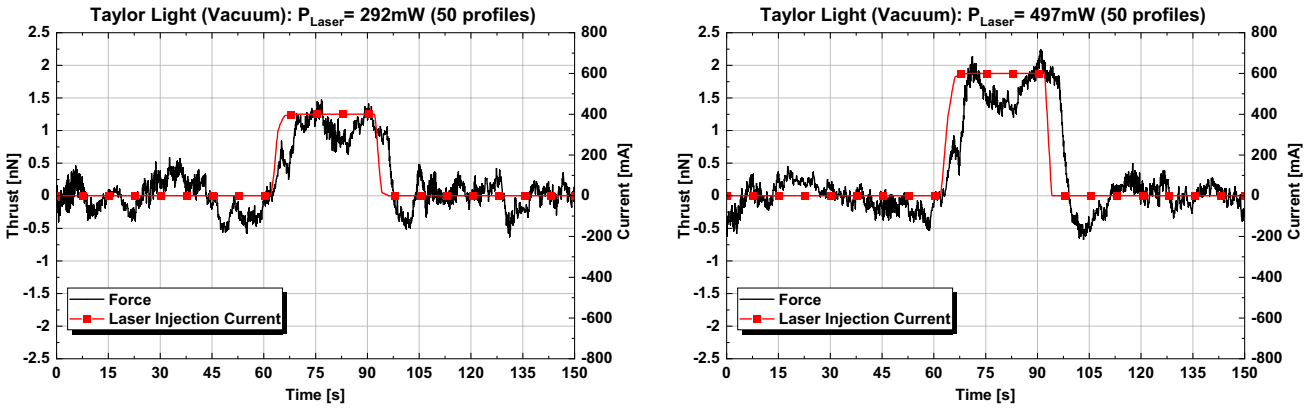

Fig. 13 Thrust Measurements of the Taylor-Light Setup

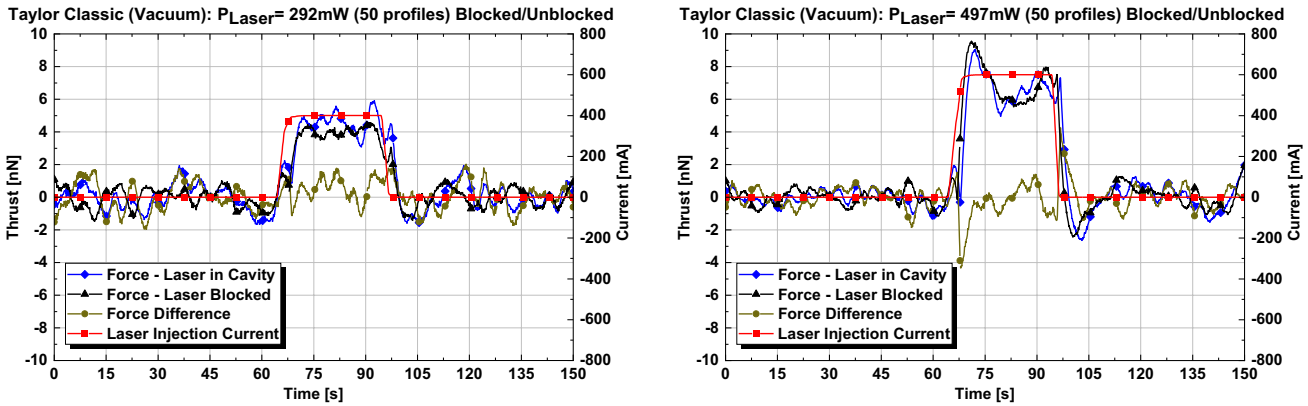

Fig. 14 Thrust Measurements of the Taylor-Classic Setup

that the fiber was intact with low losses. However, we noticed some elastic plastic material on which the coil was spun. The manufacturer could not tell us if this was vacuum compatible and there was the risk that this elastic material could rupture during evaporation, which could damage the fiber. We therefore decided to do this test at ambient pressure. The laser was powered using the liquid metal contacts and therefore we expected an influence in the Nanonewton range as with the Taylor-Classic setup. However, as the number of windings were at least 4000, thrusts in the µN range were expected according to QI. The coil had a radius of 80 mm, and we placed an aluminium metal plate of dimensions $400 \times 140 \times 10$ mm^3 at a distance of the radius away from the coil. By performing measurements with and without this Unruh-shield, a net QI thrust was expected. This differential measurement also eliminated our constant offset from the liquid metal feedthroughs.

Figure 15 (Left) shows the actual setup of the coil on the balance. Table 5 gives a summary of all our measurements, where we used the average power between input and output for the actual force prediction. Indeed, for the no-shield configuration, we measured again a few Nanonewtons offset, as this semiconductor laser used similar currents compared to the diode laser in the Taylor-Classic setup. However, this value was independent of the fact if a metal Unruh-shield was present or not. Taking the difference gives a null result as shown in Fig. 16 for two power levels.

The asymmetric loop used the battery-powered laser with Bluetooth control without any feedthrough issues. As we made the coil ourselves with known materials, the test could be done again in vacuum. The complete setup is shown in Fig. 15 (Right). As summarized in Table 5, also here, no thrust was seen at all independent of the configuration with the asymmetric coil alone or with the Unruh shield next to the smaller or larger radius. We even decreased the metal shield distance to 10 mm away from the coil without seeing any difference. An example of the thrust measurement with or without the Unruh shield at the big radius is shown in Fig. 17.

These measurements rule out anomalous thrust predictions by 4 orders of magnitude for the average power levels used.

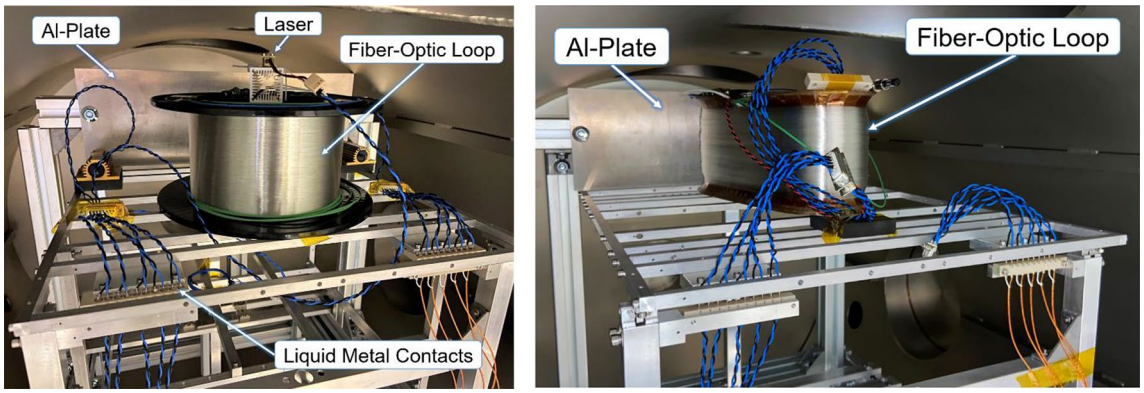

Fig. 15 Fiber-Optic Loops (Left: Symmetrical Loop positioned on the Thrust Balance with an Artificial Unruh-Shield, Right: Asymmetrical Loop with an Artificial Unruh-shield facing its Larger Diameter)

Table 5 Photon-loop Measurements

Setup	Measurement Influence	Windings (S)	Unruh Shield	Average Fiber Power (P)	QI Force Prediction (F = PS/c)	Measured Thrust
Symmetric Loop	Liquid metal contacts	> 4000	No	31 mW	0 nN	(2.64 ± 1.42) nN
				210 mW	0 nN	(6.41 ± 1.28) nN
			Yes	31 mW	420 nN	(2.62 ± 1.27) nN
				210 mW	2809 nN	(6.91 ± 1.44) nN
	None (Differential)	> 4000	Differential	31 mW	420 nN	(0.02 ± 1.42) nN
				210 mW	2809 nN	(0.50 ± 1.44) nN
Asymmetric loop	-	> 3300	No	31 mW	341 nN	(0.02 ± 0.23) nN
				203 mW	2234 nN	(0.08 ± 0.26) nN
			At Small Radius	31 mW	> 341 nN	(0.09 ± 0.33) nN
				203 mW	> 2234 nN	(0.02 ± 0.34) nN
			At Big Radius	31 mW	> 341 nN	(0.09 ± 0.31) nN
				203 mW	> 2234 nN	(0.10 ± 0.39) nN

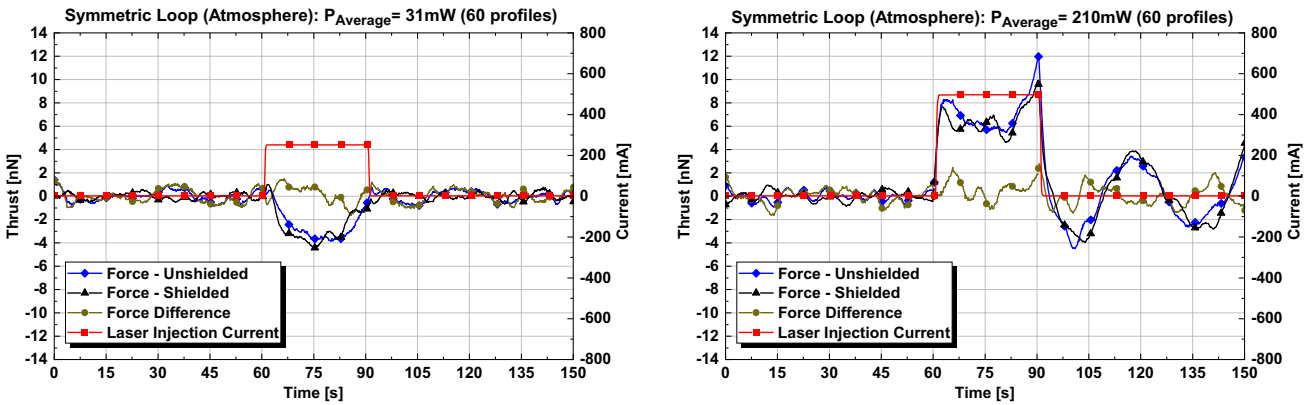

Fig. 16 Difference in Measured Thrust Values in the Presence and Absence of an Unruh-Shield for the Symmetric Loop at Ambient Pressure (Influence of Liquid Metal Contacts)

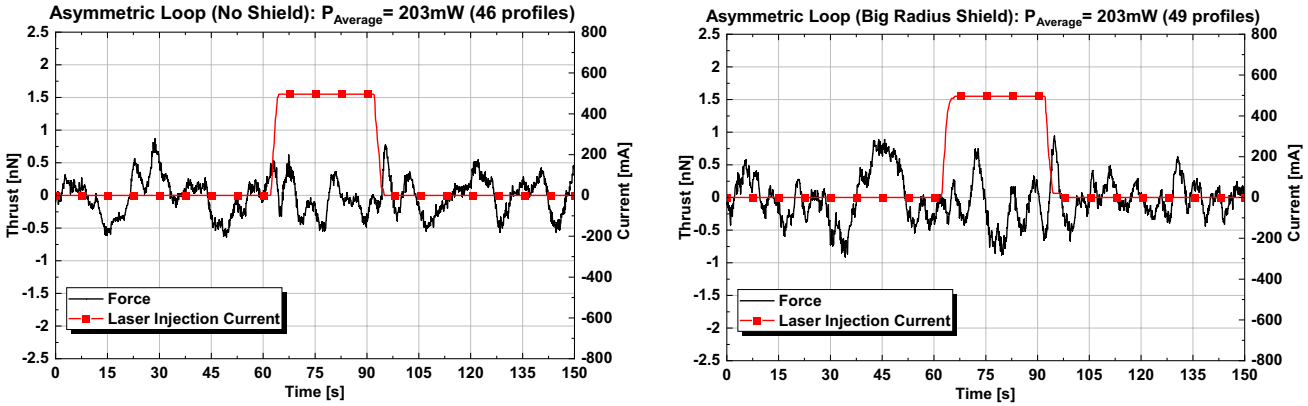

Fig. 17 Thrust Measurements of the Asymmetric Loop in Vacuum without and with Unruh Shield facing the Big Radius of the Loop

4 Conclusion

We performed an extensive investigation of detecting any anomalous thrust from laser resonators and photon-loops that were motivated by McCulloch's QI theory, which suggests that photons are fast enough to interact with their environment. To produce thrust, either mass asymmetry such that the environment-interaction on either side are not equal, or a geometric asymmetry for different photon accelerations on both ends is believed to be necessary.

Key to our search was the development of a thrust balance that eliminated all known thermal and electromagnetic interactions to such an extent, that a resolution was possible below the photon thrust limit. This is equivalent to the classical radiation pressure force emitted in one direction using the input power of the device under test. Usually, this can be demonstrated with a laser as the state-of-the-art in propellantless propulsion. Any anomalous thrust must be larger than this limit to be of interest for applications.

Many different configurations were tested including metal cavities with different shapes, laser resonators as recently suggested by Taylor or symmetric and asymmetric fiber-optic coils, which were tested with and without metal shields that should have affected the photon's environment significantly. No such effect was seen in any of our setups within our resolution of photon thrust. Comparing to predictions from QI theory, anomalous forces should have been detected at least 4 orders of magnitude above. In our comparison, we always used worst-case assumptions like a minimum number of windings for our coils or no specific geometrical modifications of the thrust prediction formula, which would increase the predicted anomalous thrust even more. We used the force amplification instead of the quality factor for the resonator predictions, as we believe that this is the correct interpretation, which would otherwise add another 4 orders of magnitude of discrepancy.

Of course, one has to take into account that our simple application of QI thrust prediction must be only an assumption as in reality the actual geometry must play an important role. However, McCulloch claimed to exactly match claimed thrusts for the EMDrive and other devices with his simple equations [4, 5], which should then apply to our configurations with similar dimensions too. In any case, at least 4 orders of magnitude are a lot to take some non-ideal geometrical parameters into account. It should be no surprise that our recent measurement on the EMDrive question the good EMDrive-QI correlation as well [2]. Our setup implementation with a proper vacuum chamber, balance, laser source and typical resonators or fiber-optic coils is representative for an actual implementation as it was suggested that such devices may compete with electric propulsion thrusters on satellites.

Our results rule out anomalous laser-based propellantless thrusters above classical photon thrust that were inspired by McCulloch and Taylor within our laboratory-scale geometries and power levels up to approximately one Watt. This puts strong limits also on other theories and designs that are based on these concepts.

Acknowledgements We gratefully acknowledge the support from DARPA DSO under award number HR001118C0125 and discussions with M. McCulloch. The quick supply of the semiconductor laser by LUMILOOP was greatly appreciated.

Funding Open Access funding enabled and organized by Projekt DEAL.

7. References

1. Shawyer, R.: Second generation EmDrive propulsion applied to SSTO launcher and interstellar probe. Acta Astronaut. **116**(October), 166–174 (2015)
2. M. Tajmar, O. Neunzig, and M. Weiker, "High-Accuracy Thrust Measurements of the EMDrive and Elimination of False-Positive Effects," in *Proceedings of the Space Propulsion Conference*, 2021, p. SP2020_268.
3. Taylor, T.S.: Propulsive forces using High-Q asymmetric high energy laser resonators. J. Br. Interplanet. Soc. **70**(7), 238–243 (2017)
4. Mcculloch, M.E.: Can the emdrive be explained by quantised inertia? Prog. Phys. **11**(1), 78–80 (2015)
5. McCulloch, M.E.: Testing quantised inertia on emdrives with dielectrics. Europhys. Lett. **118**(3), 34003 (2017)
6. McCulloch, M.E.: Inertia from an asymmetric Casimir effect. EPL **101**(5), 2013 (2013)
7. Bae, Y.K.: Photonic laser propulsion: proof-of-concept demonstration. J. Spacecr. Rockets **45**(1), 153–155 (2008)
8. Bae, Y.K.: Photonic laser thruster: 100 times scaling-up and propulsion demonstration. J. Propuls. Power **2020**, 1–8 (2020)
9. D. Hambling (2021) The EmDrive just won't die. Popular Mechanics. https://www.popularmechanics.com/space/rockets/a33917439/emdrive-wont-die/. Accessed 29 Jan 2021.
10. M. McCulloch (2021) LEMdrive?. http://physicsfromtheedge.blogspot.com/2016/07/lemdrive.html. Accessed 29 Jan 2021.
11. Polk, J.E., et al.: Recommended practice for thrust measurement in electric propulsion testing. J. Propuls. Power **33**(3), 539–555 (2017)
12. M. McCulloch (2020) Physics from the Edge Blog. http://physicsfromtheedge.blogspot.com/.